

A multifrequency study of giant radio sources

III. Dynamical age vs. spectral age of the lobes of selected sources

J. Machalski^{1*}, M. Jamrozy¹ and D.J. Saikia²

¹ *Obserwatorium Astronomiczne, Uniwersytet Jagielloński, ul. Orła 171, 30244 Kraków, Poland*

² *National Centre for Radio Astrophysics, TIFR, Pune University Campus, Post Bag 3, Pune 411 007, India*

Accepted. Received

ABSTRACT

The dynamical ages of the opposite lobes of selected giant radio sources are estimated using the DYNAGE algorithm of Machalski et al., and compared with their spectral ages estimated and studied by Jamrozy et al. in Paper II. As expected, the DYNAGE fits give slightly different dynamical ages and other model's parameters for the opposite lobes modelled *independently* each other, e.g. the age ratios are found between ~ 1.1 to ~ 1.4 . Demanding similar values of the jet power and the radio core density for the same source, we look for a *self-consistent* solution for the opposite lobes, which results in different density profiles along them found by the fit. We also show that a departure from the equipartition conditions assumed in the model, justified by X-ray observations of the lobes of some nearby radio galaxies, and a relevant variation of the magnetic-field strengths may provide an equalisation of the lobes' ages. A comparison of the dynamical and spectral ages shows that a ratio of the dynamical age to the spectral age of the lobes of investigated giant radio galaxies is between ~ 1 and ~ 5 , i.e. is similar to that found for smaller radio galaxies (e.g. Parma et al. 1999). Supplementing possible causes for this effect already discussed in the literature, like uncertainty of assumed parameters of the model, an influence of a possible departure from the energy equipartition assumption, etc., the further two are pointed out and discussed: (i) a difference between the injection spectral indices describing the initial energy distributions of the emitting relativistic particles determined using the DYNAGE algorithm in the dynamical analysis and in the classical spectral-ageing analysis, and (ii) a different influence of the axial ratio of the lobes in estimation of the dynamical age and the spectral (synchrotron) age. Arguments are given to suggest that DYNAGE can better take account of radiative effects at lower frequencies than the spectral-ageing analysis. The DYNAGE algorithm is especially effective for sources at high redshifts, for which an intrinsic spectral curvature is shifted to low frequencies.

Key words: galaxies: active – galaxies: evolution – galaxies: kinematics and dynamics

1 INTRODUCTION

There are several approaches to estimate the age of a classical double radio source, beginning with a use of the projected linear size of that source and estimating the speed of its expansion to that size. Direct measurements of the expansion speed inferred from the proper motions of the hot spots in compact symmetric radio sources gave values of about $0.2c$ – $0.3c$ (cf. Owsianik, Conway & Polatidis 1998; Owsianik & Conway 1998). An extrapolation of these motions back

in time indicates very young ages of such sources, being of the order of 10^2 – 10^4 years. On the other hand, all the analytical models of the dynamics and radio-emission properties of powerful double-lobed radio sources (e.g. Scheuer 1974; Begelman & Cioffi 1989; Falle 1991; Nath 1995; Kaiser, Dennett-Thorpe & Alexander 1997; Blundell, Rawlings & Willott 1999; Manolakou & Kirk 2002; Kino & Kawakatu 2005) predict that those speeds reduce gradually by an order of magnitude or even more with the source age.

The above has been confirmed by the classical spectral-ageing analysis. There is no doubt that radio continuum spectra in different parts of an extended radio source contain important information about the various energy losses

* E-mail: machalsk@oa.uj.edu.pl (JM); jamrozy@oa.uj.edu.pl (MJ); djs@ncra.tifr.res.in (DJS)

and gains of the radiating particles during the lifetime of the source. With the assumptions that (i) these particles are immersed in a uniform magnetic field, (ii) they are not significantly reaccelerated within the source (their lobes), and (iii) there are no significant mixing of new and old particles – the observed radio spectrum should steepen with increasing distance from the place of the last acceleration, i.e. from the hot spots. These predictions have been detected in many radio sources and used to estimate the radiative ages of the emitting particles and the expansion speeds in several samples of powerful 3CR sources (e.g. Myers & Spangler 1985; Alexander & Leahy 1987; Leahy, Muxlow & Stephens 1989; Carilli et al. 1991; Liu, Pooley & Riley 1992), in samples of low-luminosity and medium-luminosity radio galaxies (e.g. Klein et al. 1995; Parma et al. 1999), as well as in samples and/or of individual ‘giant’-sized radio sources (e.g. Lacy et al. 1993; Saripalli et al. 1994; Mack et al. 1998; Schoenmakers et al. 1998, 2000; Lara et al. 2000).

However, the observed steepening of the spectrum need not be entirely due to radiative energy losses. A possible evolution of the local magnetic fields, a bulk backflow and significant mixing of the lobe material, or the difficulties in disentangling the effects of the various loss processes have been pointed out in a number of papers (cf. Rudnick, Katz-Stone & Anderson 1994; Eilek & Arendt 1996; Jones, Ryu & Engel 1999). The spectral steepening due to the energy losses is parameterised by a single ‘break’ in the observed spectrum, ν_{br} . The spectral age of the particle population with the observed ν_{br} within a constant magnetic field of strength B is proportional to $B^{-3/2}\nu_{\text{br}}^{-1/2}$. If B decreases while the source (its lobes) expands, the spectral age should overestimate the true age of the source. However this age is usually found to be lower than the source’s age inferred from the dynamical considerations (cf. Kaiser 2000, hereafter referred to as K2000).

For the first time the problem of how to reconcile the spectral and dynamical ages was undertaken by Blundell & Rawlings (2000). They discussed how these two can be quite discrepant from one another rendering use of the classical spectral ageing method inappropriate. Moving beyond the traditional bulk backflow picture and considering alternative means of the transport of high-energy particles, the authors explained the spectral steepening along the lobes not predominantly by synchrotron ageing but by gentle gradients in the magnetic field. They contended that spectral ages can give meaningful estimates of dynamical ages only when these ages are less or much less than 10^7 years. The same problem was studied by K2000 who extended the spectral-ageing methods including the underlying source dynamics into the age estimates. The author claimed that if the bulk backflow and energy losses of the relativistic electrons, both radiative and adiabatic, are self-consistently taken into account, the discrepancies between spectral ages and dynamical ages arising from the earlier methods can be resolved. However analysing the K2000 model, Machalski et al. (2007) realised that in a majority of the extended FR II-type radio sources – even those without distorted lobe structures – the surface-brightness profiles are far from the expected smooth shapes, making the fitted free parameters of the model highly uncertain. Besides, the K2000 method requires rather high-resolution observations of the radio lobes. But usually high-resolution observations of low-brightness sources cause a se-

rious loss of the flux density, so that the K2000 method can in fact only be applied to the strongest sources such as Cyg A.

In Jamrozy et al. (2008, Paper II of this series), multifrequency observations with the Very Large Array (VLA) and the Giant Metrewave Radio Telescope (GMRT) (Konar et al., 2008, Paper I of this series) have been used to determine the spectral ages of ten selected giant-sized radio galaxies (GRGs). Using the classical spectral-ageing approach and applying two different formulae for the equipartition magnetic field estimates: the classical formula of Miley (1980) and the revised formula of Beck & Krause (2005) – the spectral age distributions along the main axis of the lobes were analysed. In that paper we found that practically the statistics of the derived age is independent of the equipartition field formula applied, though those ages can be quite different for individual sources. We also analysed the injection spectral indices characterising an initial power-law energy distribution of the emitting particles. Those indices, determined by fit to the observed radio spectra with the SYNAGE algorithm of Murgia (1996) were found to be correlated either with luminosity or redshift, as well as with linear size of the source.

In this paper dynamical ages of the lobes of the ten GRGs studied in Paper II are determined and compared with their spectral ages. Using the DYNAGE algorithm (Machalski et al. 2007), we derive the age, the average expansion velocity of the lobes’ heads, the *effective* injection spectral index which approximates the initial electron continuum averaged over a very broad energy range and over the present age of source, and other dynamical properties of the sources like their jets’ power, central density near the radio core which determines the local environment density in which the jets propagate, and the internal pressure in the lobes. In Section 2 we describe briefly the DYNAGE algorithm for fitting the dynamical parameters of the model to the observational data given in Section 3. In Section 4 we present the results of the fit, while the discussion of the results, especially of the two factors causing a difference between the dynamical and the spectral ages are given in Section 5.

2 THE DYNAGE ALGORITHM

This algorithm is an extension of the analytical model for the evolution of FR II-type radio sources combining the dynamical model of Kaiser & Alexander (1997) with the model for expected radio emission from a source (its lobes or cocoon) under the influence of energy loss processes published by Kaiser, Dennett-Thorpe & Alexander (1997, hereafter KDA model). One of the basic assumptions of the KDA model is a *continuous* delivery of kinetic energy from the active galactic nucleus (AGN) to the radio lobes through the jets (e.g. Falle 1991). The jets terminate in strong shocks where the jet particles are accelerated and finally inflate the cocoon. The density distribution of unperturbed external gas is approximated as

$$\rho(r) = \rho_0 \left(\frac{r}{a_0} \right)^{-\beta}; \quad \text{for } r \geq a_0, \quad (1)$$

where ρ_0 is the central density at the core radius a_0 , and the exponent β describes the density profile in the simplified King's (1972) model. Such a distribution of the ambient medium is assumed to be invariant with redshift. As in KDA, the lobe (i.e. half of the cocoon) is approximated by a cylinder of length D and base diameter b , so that its volume V_c is determined via the axial ratio, $R_T = D/b$. The cocoon expands along the jet axis driven by the hotspot plasma pressure p_h and in the perpendicular direction by the cocoon pressure p_c . The ratio of these pressures is constant for a given radio lobe and depends on its R_T . In our calculations we use the empirical formula taken from K2000

$$p_{hc} \equiv p_h/p_c = (2.14 - 0.52\beta)R_T^{2.04-0.25\beta}.$$

Thus the model predicts a self-similar expansion of the cocoon (lobe) and gives analytical formulae for the time evolution of its geometrical and physical parameters, e.g. the length of the lobe

$$L(t) = c_1 \left(\frac{Q_{\text{jet}}}{\rho_0 a_0^\beta} \right)^{1/(5-\beta)} t^{3/(5-\beta)}, \quad (2)$$

and the cocoon pressure

$$p_c(t) = \frac{18c_1^{(2-\beta)}}{(\Gamma_x + 1)(5-\beta)^2 \mathcal{P}_{hc}} (\rho_0 a_0^\beta)^{3/(5-\beta)} \times Q_{\text{jet}}^{(2-\beta)/(5-\beta)} t^{-(4+\beta)/(5-\beta)}, \quad (3)$$

where c_1 is a dimensionless constant, Γ_x – the adiabatic index of unshocked medium surrounding the cocoon (lobe), t – the time elapsed since the jet started from the AGN, i.e. it is the source's (here its lobes') actual age. The cocoon's pressure determines the energy density within it via the adiabatic index Γ_c of the cocoon as a whole, depending on the relative pressures of relativistic electrons, thermal particles, and magnetic 'fluid'

$$u_c(t) = p_c(t)/(\Gamma_c - 1),$$

where $u_c = u_B + u_e(1+k')$, with the equipartition condition

$$\xi \equiv \frac{u_B}{u_e(1+k')} = \frac{1+p}{4} = \frac{\alpha_{\text{inj}} + 1}{2}, \quad (4)$$

where k' is the ratio of the energy density of thermal particles to that of the electrons, and p is the power index of the power-law energy spectrum of radiating particles. The magnetic field (assumed to be completely tangled) with the energy density u_B and adiabatic index Γ_B satisfied the relation

$$B(t) \propto u_B^{1/2}(t) \propto t^{-\left[\frac{(4+\beta)\Gamma_B}{2(5-\beta)\Gamma_c}\right]}. \quad (5)$$

As in KDA, we assume that the jets consist of an electron-positron plasma and that the energy contribution from relativistic protons is completely negligible.

The above dynamical equations are supplemented with an integral giving the total radio emission from the cocoon at a frequency ν . The cocoon is split into many small volume elements δV , each of which is allowed to evolve by expanding adiabatically, i.e. changing the pressure from the hotspot pressure $p_h(t_i)$ to the cocoon pressure $p_c(t_i)$ as a function of injection time t_i . Tracing the effects of adiabatic expansion, synchrotron losses (with the assumed effective isotropisation of the particles' pitch angle distribution), and inverse

Compton scattering on the cosmic background radiation in the volume elements independently, the radio power of the cocoon P_ν at a fixed observing frequency is obtained by summing up the contributions from all elements, resulting in the integral over t_i (equation (16) in KDA). The integral is not analytically solvable and has to be calculated numerically.

The DYNAGE algorithm allows one to determine the values of four of the model's free parameters, i.e. the jet power, Q_{jet} , central core density, ρ_0 , injected spectral index, α_{inj} , and dynamical age, t . The determination of their values is possible by the fit to the observational parameters of a source: its projected linear size, D , the volume of the cocoon, V_c , the radio luminosity, P_ν , and the radio spectrum, α_ν , which provides P_{ν_i} at a number of observing frequencies $i = 1, 2, 3 \dots$

The values of several free parameters of the model have to be assumed. The assumed values are listed in Table 1, where $\gamma_{i,\text{min}}$ and $\gamma_{i,\text{max}}$ are the Lorentz factors determining the energy range of the relativistic particles used in integration of their initial power-law distribution. Since there is a mixture of three different fluids in the cocoon, this is likely that its equation of state varies within the cocoon and with time. In the present calculations we choose the KDA 'Case 2' where the cocoon's mixed material has a non-relativistic equation of state but the energy density of the magnetic field is proportional to that of the relativistic particles. As discussed in KDA, in this case the value of ξ increases with time which implies that after some time u_B starts to dominate the total energy density in a given volume element δV . However at the same time the total volume of the cocoon increases by a much larger factor, so that the approximation of the adiabatic index of the whole cocoon of 5/3 is justified. The calculations show that the model fits obtained either with $\Gamma_c=5/3$ or $\Gamma_c=4/3$ is negligible if k' is kept constant. More pronounced is influence of a value of k' itself. An increase of k' from zero to ten causes a $\sim 10\%$ to $\sim 20\%$ increase of the age due to a thermal expansion of the lobes (for the largest values of R_T it can be more than 30%, cf. Machalski et al. 2008). This effect, though ruling the entire time scale, does not affect age differences between the opposite lobes (as far as k' values are comparable in both lobes). However, without an independent evidence about the fractional content of thermal particles, holding its value as zero seems to be acceptable when we analyse the above differences.

Furthermore, we assume the orientation of the jet axis to the observer's line of sight, θ . Because of the giant linear sizes of the investigated sources, we assume $\theta = 90^\circ$ for almost all the lobes except two for which the observed asymmetries in the lobes' separation and/or in their brightness suggest $\theta < 90^\circ$. The details are given in Section 3. An extensive discussion of limitations of the DYNAGE method and dependence of the age solution on the assumed values of the model's free parameters are given in Machalski et al. (2007). For example, changing the value of $\gamma_{i,\text{min}}$ from 1 to 10 decreases the age of a source (lobe) by about 2%–5%, while varying the value of a_0 between 20 kpc and 5 kpc changes the age from about -10% to about $+20\%$, which is not larger than the age uncertainties determined for the GRGs analysed in this paper (cf. Table 3).

The fitting procedure consists of three steps:

(1) For a given value of α_{inj} and a number of values of t , the values of $Q_{\text{jet}}(\alpha_{\text{inj}}, t, P_\nu)$ and $\rho_0(\alpha_{\text{inj}}, t, P_\nu)$ are deter-

Table 1. Assumed values of the model free parameters

a_0	β	$\gamma_{i,\min}$	$\gamma_{i,\max}$	Γ_c, Γ_x	Γ_B	k'	θ
10 kpc	1.5	1	10^7	5/3	4/3	0	90°

mined by the fit of equation (2) to the deprojected linear size of a lobe $D/\sin\theta$ and equation (16) of KDA to the lobe's luminosity at a given frequency P_ν .

(2) Performing the above procedure for all of the luminosities chosen to represent the lobe's spectrum, we get a set of solutions for Q_{jet} and ρ_0 shown in Fig. 1a. As the source (its lobe) must have the same age at any of the observing frequencies, we search for an age at which the parameters Q_{jet} and ρ_0 have possibly identical values. A perfect intersection of all the $Q_{\text{jet}} - \rho_0$ curves corresponding to different observing frequencies at some particular age is expected if the observed spectrum agrees with the theoretically predicted one in the framework of the 'continuum injection' (C.I.) model of energy losses (cf. Myers & Spangler 1985; Carilli et al. 1991). However, the observed spectrum of the analysed sources (and their lobes) may depart from such a theoretical shape, therefore the 'goodness' of the intersection is quantified by the $\Delta(t)$ measure defined by equation (4) in Machalski et al. (2007). A minimum of $\Delta(t)$ (i.e. 'the best' intersection of the $Q_{\text{jet}} - \rho_0$ curves for different frequencies and for the given value of α_{inj}) is considered as an estimate of the source's (lobe's) dynamical age $t(\alpha_{\text{inj}})$ (Fig. 1b). This minimum also distinguishes a value of $Q_{\text{jet}}(\alpha_{\text{inj}})$ (and ρ_0, p_c, u_c , all dependent on a value of α_{inj}).

(3) The steps (1) and (2) are repeated for a number of α_{inj} values. By varying this parameter during the fitting procedure, we search for its value which provides a minimum of the product $Q_{\text{jet}} \times t$, i.e. a minimum of the kinetic energy delivered to the given lobe during the age t . Following the original KDA assumption during integration of the expected radio emission, the minimum energy condition is initially fulfilled in each volume element of the cocoon, therefore the minimum of $Q_{\text{jet}} \times t$ corresponds to a minimum of the total energy density in it.

3 THE DATA

The observational parameters of the GRGs under investigation and their lobes are given in Table 2. Columns (1), (2), (3), and (7) are self explanatory. Columns (4) and (8) give linear size D of the opposite lobes (the first line) and their axial ratio R_T (the second line); both values with their standard error. The value of R_T is determined on the maps with the highest sensitivity to surface brightness available as the ratio of D and the largest deconvolved width of transversal cross-sections through the lobe, b . The standard errors of D and R_T result from the uncertainties of angular size of the lobe's length and its base diameter. Columns (5) and (9) give the observing frequencies selected from the available spectral data and used to calculate the radio luminosities, P_ν , necessary for the fitting procedure (cf. Section 2). For a technical reason, we limited the fitting procedure to four frequencies only, possibly spanning the largest frequency range. The letter preceding the observing frequency indicates the radio telescope (array) or the radio survey with (or in) which

a relevant flux density was measured: G – for GMRT, V – for VLA, and W – for WSRT. Mostly the flux densities published in Paper I are used, but when necessary, the spectral data are supplemented with flux densities taken from other observations (surveys): VLSS (Cohen et al. 2007), 7C (Pooley et al. 1998; Riley et al. 1999), WENSS (Rengelink et al. 1997), B3 (Ficarra et al. 1985), and NVSS (Condon et al. 1998). Where the available radio maps make it possible, the flux densities of the lobes used to calculate their luminosities are cleared of the hot spots' emission. Columns (6) and (10) give the derived luminosities calculated using $H_0=71 \text{ km s}^{-1} \text{ Mpc}^{-1}$, $\Omega_m=0.27$, and $\Omega_{\text{vac}}=0.73$.

4 DYNAMICAL AGE AND OTHER PHYSICAL PARAMETERS

4.1 Independent solutions for the individual lobes

In the first step of modelling the age and other physical parameters of the investigated GRGs, we fit them independently for each of the two lobes of a given source using their observational data given in Table 2 and the values of other free parameters of the model from Table 1, in particular with $\beta=1.5$. The dependence of the resulting model solutions of $t, Q_{\text{jet}}, \rho_0$, and $Q_{\text{jet}} \times t$ on α_{inj} for the N-lobes of J0912+3510 and J1155+4029, i.e. for these lobes for which we assumed $\theta < 90^\circ$, is shown in Fig. 2. The vertical line and the arrow indicate the value of α_{inj} that corresponds to the minimum of the kinetic energy delivered to the given lobe by the jet. The parameter values resulting from the fits are listed in columns (3)–(7) in Table 3.

As might be expected, the DYNAGE solutions of age and other physical parameters for the opposite lobes of the same source appear somewhat different. The question is whether these differences are statistically significant. To answer this question, we estimate an error on the fitted values of a given parameter. The error estimates for the fitted values of α_{inj} and age (t) of the lobes are included in Table 3. These errors indicate that a difference between the ages of the opposite lobes is always insignificant; however there is a marginal tendency of the larger lobes to be older than the opposite shorter ones. It is also worth noting that in at least three of the ten sources, a difference between the values of the effective initial spectral index α_{inj} is larger than $2.5-3\sigma$. Such differences are possible if an evolution of the magnetic field, various energy losses and acceleration processes of the relativistic particles, and mixing of plasma at different ages – are different at the heads of the opposite lobes.

The above suggests that such differences in the ageing properties of the opposite lobes, especially in giant-sized radio sources, may be caused by different environmental conditions. This is likely confirmed by the evident differences in the fitted values of ρ_0 . Although this parameter denotes a density of the central radio core, in the DYNAGE algorithm we fit the term $\rho_0 a_0^{\beta}$ which appears in Eqs. (1), (2), and (3). If the values of a_0 and β are fixed, the fitting procedure gives the values of ρ_0 slightly or significantly different for the opposite lobes. However, we can expect a single value of ρ_0 (and Q_{jet}) for a given source. Therefore, in the next subsection we describe and check a 'self-consistent' solution for the investigated lobes.

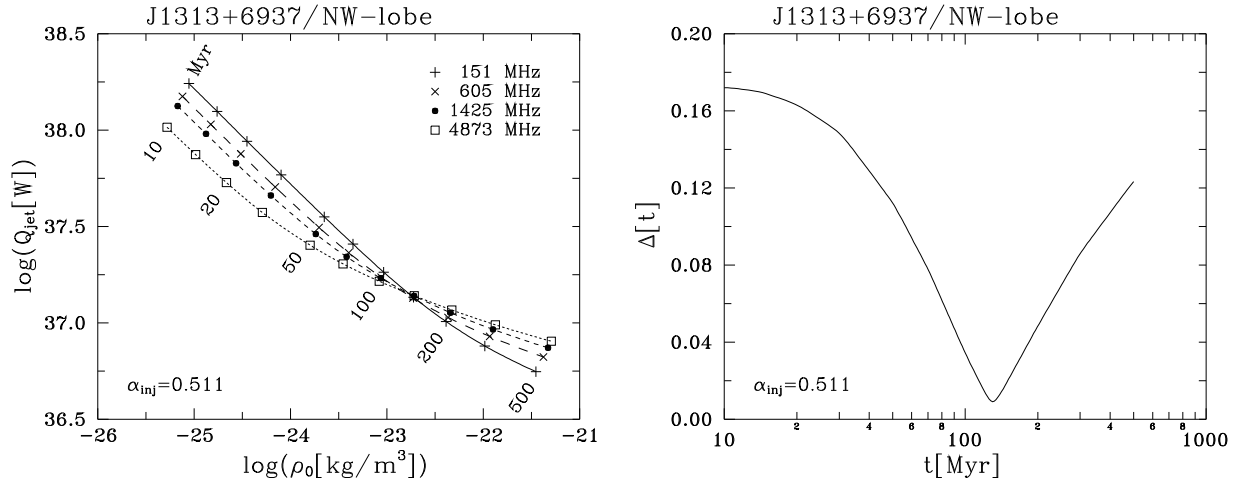


Figure 1. a) $Q_{\text{jet}} - \rho_0$ diagram for the NW lobe of J1313+6937. The radio luminosities at the four frequencies indicated and used to fit the model are given in Table 2. The α_{inj} value for which the jet kinetic energy achieves a minimum is given. b) ‘Goodness’ of fit quantified by the Δ measure vs. the age for the same value of α_{inj} . Its minimum indicates the age solution for the given lobe, cf. Table 3.

4.2 Self-consistent solution for the opposite lobes

In this second step of the modelling we averaged the values of Q_{jet} and ρ_0 found from fits for the opposite lobes (given in columns (5) and (6) of Table 3), and now treat them as the fixed free parameters of the model, $\langle Q_{\text{jet}} \rangle$ and $\langle \rho_0 \rangle$, respectively. Given these values, we can determine a value of β for each of the two opposite lobes, hereafter denoted as $\beta_{\text{s.c.}}$. In order to do that, we assume that a power-law density profile of the ambient environment can be extended to distances as large as lengths of the lobes of GRGs. Although such an assumption can be invalid for distances larger than a few hundred of kpc (cf. Gopal-Krishna & Wiita 1987; Machalski et al. 2008), the ambient densities, ρ_a , calculated for the investigated GRGs from equation (1) with $r = D$ are still within an acceptable range of density ($\sim 3 \times 10^{-28}$, $\sim 2 \times 10^{-25} \text{ kg m}^{-3}$). Thus, equalising ρ_a values in the independent solution and the self-consistent solution, we have from equation (1)

$$\beta_{\text{s.c.}} = \frac{\log(\langle \rho_0 \rangle / \rho_a)}{\log(D/a_0)},$$

and transforming equation (2) we calculate an expected age of a given lobe (in the frame of the self-consistent solution) from

$$t_{\text{s.c.}} = \left(\frac{D}{c_1}\right)^{(5-\beta_{\text{s.c.}})/3} \left(\frac{\langle \rho_0 \rangle a_0^{\beta_{\text{s.c.}}}}{\langle Q_{\text{jet}} \rangle}\right)^{1/3}.$$

Finally, seeking a preservation of the minimum energy conditions, we search for the relevant value of α_{inj} , hereafter denoted as $\alpha_{\text{inj}}^{(\text{s.c.})}$. The resulting values of $\beta_{\text{s.c.}}$, $\alpha_{\text{inj}}^{(\text{s.c.})}$, $t_{\text{s.c.}}$, and $(v_h/c)_{\text{s.c.}}$ which is an average expansion speed of the lobe derived from the self-consistent solution, are given in columns (8)–(11) of Table 3.

5 DISCUSSION OF THE RESULTS AND CONCLUSIONS

5.1 Ages and expansion speeds of the lobes

The DYNAGE fits imply that (i) the formal ages of the opposite lobes are somewhat different, though the difference is not large, given the errors of the fit; (ii) there is a weak trend in the sense the larger lobe is ‘older’, and (iii) the average expansion speed of the larger lobe is usually higher than that of the shorter one. The implication (ii) is consistent with predictions of the simplified kinematic model for the jets’ propagation (e.g. Longair & Riley 1979): if heads of the jets move through a uniform environment at the same speed v_h at an angle θ to the line of sight, the shorter lobe will appear younger by the time delay of $(D_1 + D_2)\cot(\theta)/c$. For the projected linear size $D_1 + D_2 = 1 \text{ Mpc}$ and $\theta \approx 70^\circ$, an age difference will be less than 1.2 Myr. Therefore the derived age differences for the opposite lobes, much higher than 1–2 Myr, cannot be related to the kinematic effects only, but they likely indicate actual different jet’s propagation conditions in the opposite directions through the galactic and/or intergalactic medium. The implication (iii) will be expected if both the lobes are of the same age. Indeed, in spite of the formal age differences, in seven out of ten GRGs a higher expansion speed is found for the larger lobe. A faster expansion, in turn, may imply a thinner environment and/or a higher jet power. Surprisingly, this is not the case for the four sources: J0912+3510, J1155+4029, J1313+6937, and J1702+4217; the core density fitted for their larger lobes is higher than that for the shorter ones. Only the shorter (and formally older) lobes of the sources: J0927+3510, J1343+3758, and J1604+3438 seem to expand slower due to a denser ambient medium at their side, however the speed differences are insignificant, being of an order of the speed errors of about $0.005c$ – $0.008c$.

The self-consistent solutions do not change the above picture radically. A median of the age quotient (older to younger) of about 1.2 is similar in both the independent solutions and in the self-consistent solutions. Still the expan-

Table 2. Observational parameters of the sources and their lobes

IAU name	z	Larger	D(kpc)	ν	$\log P_\nu$	Shorter	D(kpc)	ν	$\log P_\nu$
Other name		lobe	R_T	(MHz)	(W Hz ⁻¹ sr ⁻¹)	lobe	R_T	(MHz)	(W Hz ⁻¹ sr ⁻¹)
(1)	(2)	(3)	(4)	(5)	(6)	(7)	(8)	(9)	(10)
J0912+3510	0.2489	S	901±19	7C151	24.881	N†	578±82	7C151	24.556
			5.2±1.5	G606	24.436		4.1±1.1	G606	24.154
				V1400	24.156			V1400	23.892
				V4860	23.710			V4860	23.456
J0927+3510	(0.55)	SE	1119±20	7C151	25.395	NW	1087±32	7C151	25.253
			4.6±1.2	G606	25.005		4.4±1.2	G606	24.788
				V1400	24.711			V1400	24.486
				V4860	24.236			V4860	24.000
J1155+4029	(0.53)	SW	956±12	G241	25.346	NE‡	628±10	7C151	26.343
			8.1±1.4	G605	24.968		3.2±0.8	B408	25.925
				V1400	24.603			V1400	25.383
				V4860	24.036			V4860	24.821
J1313+6937	0.1064	SE	422±30	7C151	24.806	NW	323±29	7C151	24.942
DA340			3.3±1.1	G605	24.389		2.4±0.8	G605	24.516
				V1425	24.095			V1425	24.229
				V4873	23.593			V4873	23.759
J1343+3758	0.2267	NE	1404±36	7C151	24.409	SW	1059±11	7C151	24.716
			5.4±1.3	W325	24.200		3.3±0.7	W325	24.423
				V1400	23.811			V1400	23.981
				V4860	23.290			V4860	23.382
J1453+3308	0.249	S	756±12	G240	24.953	N	570±12	G240	25.170
B1450+333			4.8±1.6	G605	24.704		2.8±1.0	G605	24.933
				V1400	24.356			V1400	24.586
				V4860	23.705			V4860	24.029
J1604+3438	0.2817	E	443±17	G239	24.692	W	403±21	G239	24.638
			2.6±0.	G614	24.361		2.4±0.4	G614	24.300
				G1265	24.198			G1265	24.107
				V4860	23.603			V4860	23.526
J1604+3731	0.814	NW	679±23	G334	25.708	SE	667±15	G334	25.804
7C1602+376			2.4±0.5	G613	25.439		2.8±0.5	G613	25.530
				G1289	25.219			G1289	25.318
				V4860	24.544			V4860	24.697
J1702+4217	0.476	SW	663±47	W325	25.213	NE	497±47	W325	25.364
7C1701+423			3.2±0.7	G602	25.002		1.9±0.5	G602	25.144
				V1425	24.685			V1425	24.827
				V4860	24.131			V4860	24.313
J2312+1845	0.427	NE	544±34	V74	26.751	SW	512±28	V74	26.843
3C457			4.1±1.2	G334	26.177		3.4±1.1	G334	26.284
				V1425	25.615			V1425	25.738
				V4866	25.087			V4866	25.213

Notes. A letter preceding the observing frequency indicates the radio telescope (array) used: G – GMRT, V – VLA, W – WSRT, or the surveys: 7C, B3 (cf. the text). † indicates the lobe with an inclination angle of 70° assumed; ‡ indicates the lobe with an inclination angle of 50° assumed. The corresponding values of R_Θ give the ratio of deprojected length of the lobes.

sion speeds tend to be higher for the larger lobes. Again the exception seems to be J1604+3731. The values of $\beta_{s.c.}$ found by the fits are within an acceptable range (1.38, 1.76). It is worth noting that these values are always less than 2 which is the necessary condition for forming the head of the jet and to observe a source of the FR II type. On the other hand, the self-consistent solutions require a larger difference between the effective injection spectral index $\alpha_{inj}^{(s.c.)}$ for the opposite lobes, than those found in the frame of the independent solutions. The question whether it really reflects different physical conditions governing the initial energy distribution of the relativistic particles at the head of the lobes, or it is mostly related to an uncertainty of the fit and/or wrong assumptions in the model, is open.

Another alternative self-consistent solution is plausible in which the age of the opposite lobes has to be the same,

and any differences between their size and luminosity are due to an inhomogeneity (asymmetry) in density distribution of the surrounding gaseous environment. Again, there is rather no physical circumstances for significant differences between the jet power and the central core density in the opposite directions along the jets' axis. In such a scenario, either the same values of ρ_0 , Q_{jet} , and t would be assumed for both lobes or only postulated, while the values of a_0 , β , and α_{inj} , different for the two lobes, are determined by the fit. Rearrangement of equation (2) and substitution of D for $L(t)$ gives

$$t = \left(\frac{D}{c_1}\right)^{(5-\beta)/3} \left(\frac{\rho_0 a_0^\beta}{Q_{jet}}\right)^{1/3}.$$

Applying this equation separately for either lobe of a source and demanding equality of their age, jet power, core density,

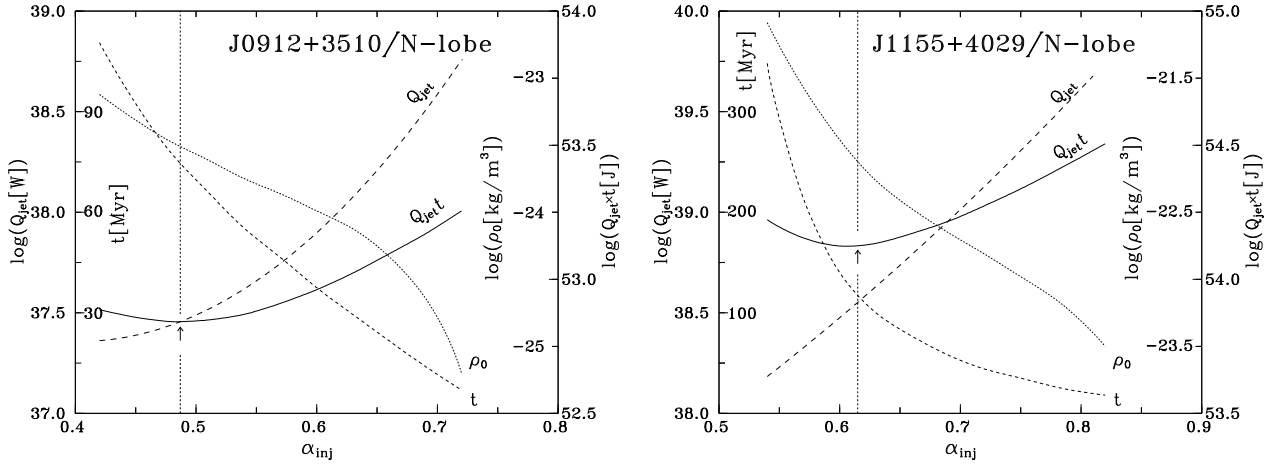


Figure 2. The dependence of jet power, Q_{jet} , age of the lobes, t , central core density, ρ_0 , and kinetic energy delivered to the lobes during the time t , $Q_{\text{jet}} \times t$ on the effective initial spectral index, α_{inj} , for the N-lobes of two different GRGs from Table 2. The minima of the kinetic energy corresponding to the ‘best solution’ of the age and other physical parameters of the given lobe are marked with the arrows. The vertical dotted lines indicate proper y-intercepts of each of the four functions $y = f(\alpha_{\text{inj}})$.

Table 3. Fitted physical parameters of the lobes. Columns from (3) to (7) give results of the independent solution, while columns from (8) to (11) give results of the self-consistent solution

Source	Lobe	α_{inj}	t (Myr)	$\log Q_{\text{jet}}$ (W)	$\log \rho_0$ (kg m^{-3})	v_{h}/c	$\beta_{\text{s.c.}}$	$\alpha_{\text{inj}}^{(\text{s.c.})}$	$t_{\text{s.c.}}$ (Myr)	$(v_{\text{h}}/c)_{\text{s.c.}}$
(1)	(2)	(3)	(4)	(5)	(6)	(7)	(8)	(9)	(10)	(11)
J0912+3510	S	0.493 ± 0.006	90 ± 17	37.80	-23.30	0.033	1.45	< 0.4	(98)	(0.031)
	N	0.487 ± 0.007	75 ± 14	37.47	-23.51	0.025	1.57	0.590	66	0.031
J0927+3510	SE	0.490 ± 0.005	41 ± 4	38.55	-23.99	0.089	1.52	< 0.4	(44)	(0.083)
	NW	0.498 ± 0.005	50 ± 5	38.38	-23.90	0.071	1.48	0.550	46	0.077
J1155+4029	SW	0.570 ± 0.030	130 ± 35	38.23	-22.00	0.024	1.47	0.632	111	0.028
	NE	0.615 ± 0.019	118 ± 28	38.55	-22.13	0.017	1.54	0.569	133	0.015
J1313+6937	SE	0.508 ± 0.011	152 ± 22	37.18	-22.66	0.010	1.46	0.486	153	0.010
	NW	0.511 ± 0.011	131 ± 18	37.15	-22.80	0.008	1.55	0.523	131	0.008
J1343+3758	NE	0.461 ± 0.018	64 ± 11	37.90	-24.24	0.071	1.58	< 0.4	(69)	(0.066)
	SW	0.516 ± 0.012	94 ± 13	37.76	-23.94	0.036	1.44	0.547	87	0.039
J1453+3308	S	0.563 ± 0.006	173 ± 23	37.70	-22.35	0.014	1.40	0.550	156	0.016
	N	0.518 ± 0.013	127 ± 17	37.69	-22.92	0.015	1.71	0.544	136	0.014
J1604+3438	E	0.506 ± 0.007	86 ± 12	37.40	-23.40	0.017	1.50	0.440	90	0.016
	W	0.511 ± 0.008	93 ± 9	37.29	-23.39	0.014	1.50	0.547	89	0.016
J1604+3731	NW	0.571 ± 0.008	54 ± 8	38.62	-23.48	0.042	1.45	0.590	51	0.045
	SE	0.536 ± 0.009	41 ± 8	38.73	-23.70	0.054	1.57	0.512	43	0.051
J1702+4217	SW	0.568 ± 0.012	74 ± 15	38.06	-23.07	0.030	1.38	0.544	85	0.026
	NE	0.538 ± 0.012	62 ± 10	38.11	-23.73	0.027	1.76	0.544	70	0.024
J2312+1845	NE	0.567 ± 0.012	86 ± 21	38.58	-22.10	0.022	1.47	0.574	83	0.023
	SW	0.567 ± 0.013	76 ± 14	38.64	-22.23	0.022	1.54	0.561	79	0.021

and core radius, we have another equation involving two unknown quantities: β_1 , and β_2 , where the fraction ρ_0/Q_{jet} is eliminated

$$a_0^{(\beta_1 - \beta_2)} = \frac{(D_2/c_{1,2})^{(5 - \beta_2)}}{(D_1/c_{1,1})^{(5 - \beta_1)}}.$$

The values of two latter parameters depend on the energy distributions of particles injected into the opposite lobes and described by α_{inj} parameters and on their observed luminosities. This dependence cannot be expressed analytically, as explained in Section 2. Besides, the values of ρ_0 and Q_{jet} (as well as α_{inj}) cannot be determined independently of the unknown values of a_0 and β . Therefore, such an ‘alternative

self-consistent solution’ obviously cannot give any explicit results.

In order to prove this we attempted to find such a solution for the lobes of J0912+3510, the sample source with a rare asymmetry where the larger lobe is also much more luminous than the shorter one. Assuming for both lobes $t = 82$ Myr, which is the average of the values determined in the ‘independent solution’ (cf. Table 3), we fit the values of Q_{jet} and ρ_0 for a number of combinations of the model parameters a_0 , β and α_{inj} . The results are shown in Fig. 3, where the abscissa axis gives the core density ρ_0 scaled to the core radius $a_0 = 10$ kpc. Exploring the parameter space we notice that (i) none of physically acceptable values of these parameters can provide comparable values of Q_{jet} for the opposite

lobes (cf. the similar paper of Brocksopp et al. 2007 and their Fig. 4), and (ii) allowing different values of Q_{jet} and ρ_0 for either lobe, the assumed age value can be achieved with *any combination* of a_0 , β and α_{inj} parameters. The above calculations confirm that there is no unique ‘alternative self-consistent solution’.

There are two possible causes of different ‘dynamical age’ solutions of the opposite lobes of a FRII-type source, especially a GRG in which the effect of projection is likely to be neglected. The first cause, the most probable one, could be related to an unknown actual distribution of magnetic fields, which may depart from the equipartition conditions in a different way in either lobe. This is confirmed by X-ray imaging observations which allow measurements of electron energies of radio lobes and magnetic fields. The derived electron energy densities often exceed those of magnetic fields by a factor of a few to several dozen. For example, the ratio ξ of about 0.16 has been found in the lobes of the galaxy Cen B (Tashiro et al. 1998) and of 0.20 and 0.13 in the E lobe and W lobe of the galaxy For A (NGC 1316), respectively (Isobe et al. 2006; Tashiro et al. 2008). Our calculations show that increasing or decreasing the magnetic-field energy density, u_B , in respect to the equipartition condition (given in equation (4)) results in an increase or decrease of the fitted age, respectively, which agrees with the finding of Parma et al. (1999). For example, the four-fold increase of the ratio ξ in the N-lobe and the corresponding decrease in the S-lobe of J0912+3510 results in about 10%–15% increase or decrease of their fitted age, respectively, i.e. eliminates the age difference found with the ‘independent solution’. This is worth to emphasize that this variation of ξ is not equivalent of changing α_{inj} . In both lobes a minimum of $Q_{\text{jet}} \times t$ is still around 0.49, which strongly supports the conclusion that the minimum of the jets’ kinetic energy appearing in the age solutions is not an artefact of numerical calculations, but has a real physical meaning. The corresponding *effective* spectral index α_{inj} is always within the narrow range of $p \approx 2.0$ – 2.4 suggested by the ‘non-relativistic shock’ paradigm for the origin of non-thermal electrons within the heads of FRII-type radio sources (e.g. Blandford & Eichler 1987; Heavens & Meisenheimer 1987).

The second cause, less probable one, could be related to a multi-episod jet activity, strongly suggested by observations of double-double radio galaxies (DDRGs, e.g. Kaiser et al. 2000; Saripalli et al. 2002; Brocksopp et al. 2007). If the jet activity has been interrupted and its multiple episodes happened in opposite directions by chance, an ‘effective’ age of the lobes would be different. There is, at least, one piece of observational evidence for such a behaviour, i.e. the northern middle lobe of the galaxy Cen A which has no counterpart in its southern lobe (Morganti et al. 1999). Its spectral age of about 20–30 Myr, estimated by Hardcastle et al. (2008), is much higher than the time scale of about 10^3 yr for instabilities in the accretion processes.

5.2 A relation between the spectral age and the dynamical age

The spectral age distribution along the jets’ axes of the ten investigated GRGs was analysed in Paper II. In this subsection we compare (i) the initial spectral indices resulting from the DYNAGE and SYNAGE fits, and (ii) the dynamical ages

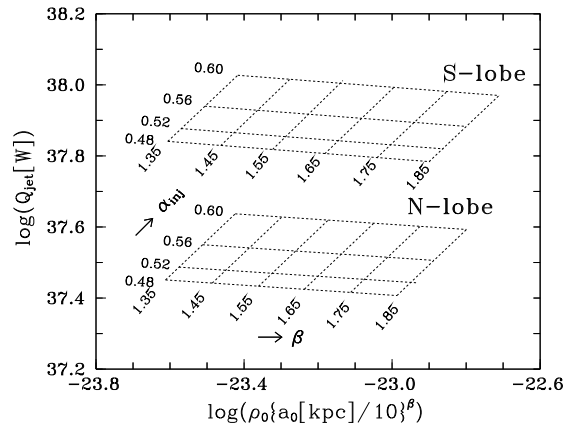


Figure 3. Model solutions for the lobes of J0912+3510 at the age of 82 Myr for both lobes. Abscissa gives the (log) core density scaled to the core radius of 10 kpc. The areas confined by dotted lines indicate very large parameter space within which both lobes would have the assumed age.

derived in this paper and the synchrotron ages analysed in Paper II and supplemented in this paper. As described in the Introduction, the notion of a spectral age of the source (or its lobes) is not explicit; it is usually considered as an age of the emitting particles which can differ in different parts of the source. Therefore in Paper II we derived two estimates of this age: the age of the oldest detected particles in the regions of the observed emission from the lobes, and the age values resulting from extrapolation of a linear regression of the age on the distance (i.e. a characteristic speed, v_{sep} , which is an indication of the speed of the lobe material relative to the hot spots) to the radio core. Besides, both these estimates were derived using two different equipartition magnetic field formulae, the classical formula of Miley (1980) and the revised formula of Beck & Krause (2005). In each case the spectral age was computed using a spectral break frequency, ν_{br} , resulting from the SYNAGE fit of the Jaffe & Perola (1973; JP) model to the radio spectrum of a given lobe for which the JP fit was mostly the best compared with those of the Kardashev-Pacholczyk (Pacholczyk 1970; KP) or ‘continuous injection’ (Kardashev 1962; CI) models.

The DYNAGE method for estimating the dynamical age of FRII-type radio sources is based on the analytical KDA model which assumes a continuous delivery of energy to the lobes through the jets with a constant power. Therefore, in order to compare the initial spectral indices resulting from the DYNAGE and SYNAGE fits, we should take into account the SYNAGE indices fitted with the CI model. However, this model of energy losses does not account for an adiabatic expansion of the cocoon, while KDA and DYNAGE do. Therefore, a model much closer to DYNAGE is the CIE model of Murgia (1996) which accounts for an adiabatic expansion of the volume of source (lobe, cocoon) and a related evolution of the magnetic field strength in the form $r(t) \propto t^k$ ($V(t) \propto t^{3k}$) and $B(t) \propto t^m$. Though each SYNAGE fit of the CIE model to the data points in the radio spectrum of a given lobe was the worst as compared with those of the JP, KP, and CI models – the resulting spectral ages, τ_{CIE} , should be closer to the dynamical ages estimated in this paper.

The break frequency for the CIE model is $\nu_{\text{br,CIE}} = (k - 2m - 1)^2 \nu_{\text{br,CI}}$. In the SYNAGE algorithm, where $k=1$ and $m=-2$, $\nu_{\text{br,CIE}} = 16 \nu_{\text{br,CI}}$ are expected for a spectrum of same initial energy distribution, the same age, and final magnetic field. However, for 20 lobes of the analysed GRGs the ratio $\nu_{\text{br,CIE}}/\nu_{\text{br,CI}}$ is consistently much less than 16, in the four sample sources is even less than 1. This is caused by a frequent large difference between α_{CI} and α_{CIE} fitted as a free parameter in SYNAGE. The values of low-frequency spectral index and break frequency for the investigated lobes, fitted with SYNAGE in the frame of CI and CIE models, as well as the values of corresponding synchrotron ages are given in Table 4. The value of magnetic field strength B_{DYN} , derived from the magnetic energy density in this paper (cf. equations (4) and (5)) and used to calculate the ages, is given in column (3). The values of α_{CI} , $\nu_{\text{br,CI}}$, α_{CIE} , and $\nu_{\text{br,CIE}}$ are given in columns (4), (5), (7), and (8), respectively. The relevant ages, τ_{CI} and τ_{CIE} , given in columns (6) and (9), respectively, are calculated from

$$\tau_{\text{CI}} = 50.3 \frac{B^{1/2}}{B^2 + B_{\text{IC}}^2} \{\nu_{\text{br,CI}}(1+z)\}^{-1/2} \text{ [Myr]}, \quad (6)$$

and

$$\tau_{\text{CIE}} = 201.2 \frac{B^{1/2}}{B^2 + B_{\text{IC}}^2} \{\nu_{\text{br,CIE}}(1+z)\}^{-1/2} \text{ [Myr]}, \quad (7)$$

where $B_{\text{IC}}[\text{nT}] = 0.318(1+z)^2$ is the inverse-Compton magnetic field strength equivalent to the cosmic microwave background radiation. Finally, the differences between the fitted low-frequency slope and the injected spectral index determined with DYNAGE, $\alpha_{\text{CI}} - \alpha_{\text{inj}}$, and $\alpha_{\text{CIE}} - \alpha_{\text{inj}}$ are given in columns (10) and (11), while the ratios between the dynamical age t derive in this paper and the synchrotron ages τ_{CI} and τ_{CIE} – in columns (12) and (13), respectively.

The data in Table 4 show that the equipartition magnetic fields derived with the DYNAGE algorithm are usually stronger than those calculated with the classical Miley's formula. On the second hand, all these fields are weaker than those calculated with the revised formula of Beck & Krause (2005) published in Paper I. The reason for the latter effect is that the observed curved radio spectra were integrated, while Beck & Krause assumed that the proton spectrum is straight and any steepening in the radio spectrum is due to energy losses of the electrons. If, however, the proton spectrum is similarly curved as the electron spectrum, the Beck & Krause values would be too high. Nevertheless, the resulting spectral ages are not too much sensitive to the magnetic field strengths, depending more on the spectral break ν_{br} and on the ratio B/B_{IC} . The examples of the spectral best fit for the lobes of two different sample sources are shown in Fig. 4. Three different fit results for the N lobes of the sources J0912+3510 and J1155+4029 are compared. Note that the quality of the fits, expressed by the reduced χ^2 values, are comparable within the frequency range for which flux-density data have been available. The fits clearly show that the frequency range crucial for a better discrimination between the models is below 100 MHz, i.e. the range where near-future observations with the LOFAR array will be decisive.

The data in Table 4 also exhibit unexpected discrepancies between the fitted values of α_{CI} (or α_{CIE}) and ν_{br} in opposite lobes of some sample sources, e.g. J1155+4029

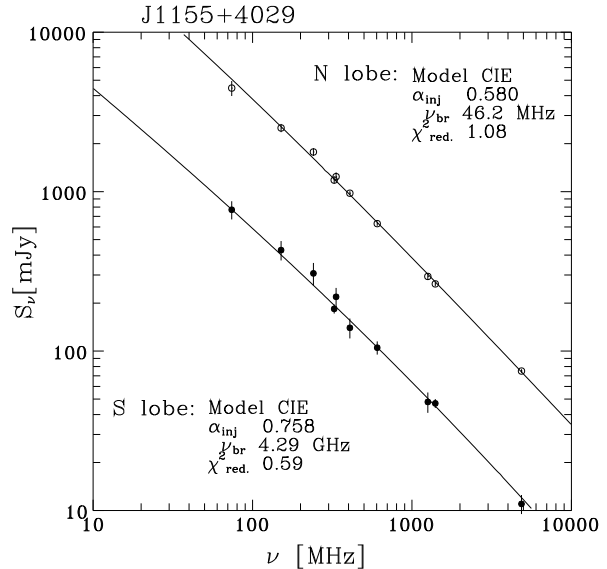


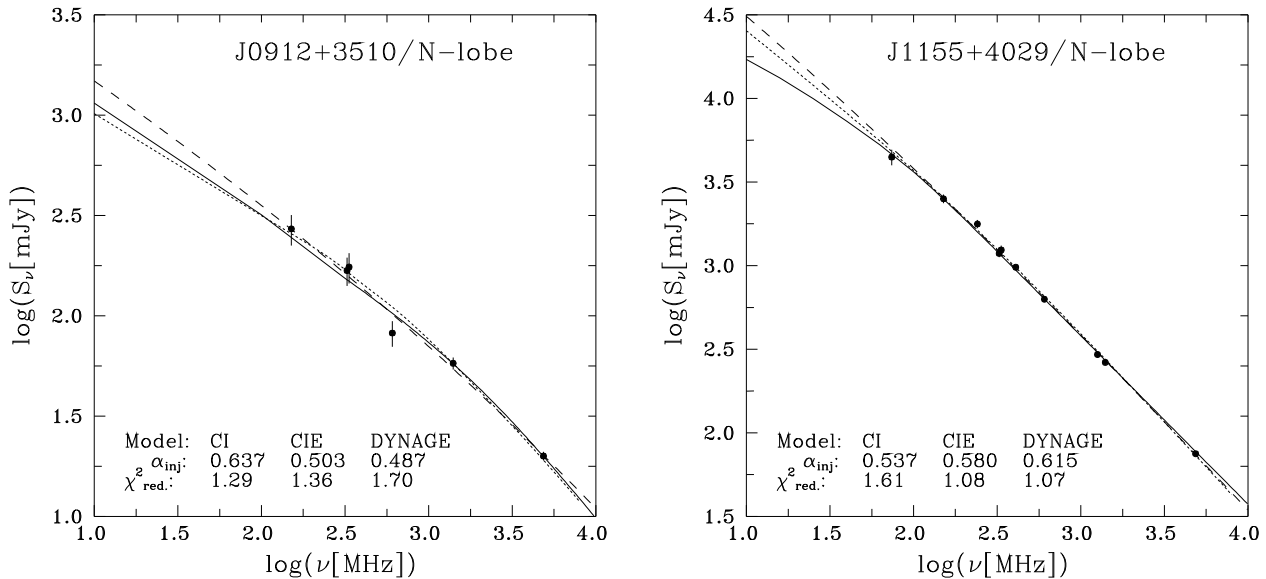
Figure 5. Radio spectra of the opposite lobes of J1155+4029 and their spectral curvature parameters fitted with the original CIE model.

and J1343+3758. The most discrepant are the values of $\nu_{\text{br,CIE}}$ in J1155+4029. This is shown in Fig. 5 where the observed spectra of its opposite lobes are compared. Both slopes and spectral shapes look very similar, nevertheless the formal fitted values of α_{inj} and especially of $\nu_{\text{br,CIE}}$ are dramatically different. How much these values are uncertain is indicated by their errors provided by SYNAGE: $32 \text{ MHz} < \nu_{\text{br,CIE}} < 241 \text{ GHz}$ and $0.08 \text{ MHz} < \nu_{\text{br,CIE}} < 1.18 \text{ GHz}$ for the SW lobe and NE lobe, respectively. This is worth to notice that J1155+4029 has the largest asymmetry in the lobes' luminosities.

The fit results indicate that a difference between the dynamical age, t , and the synchrotron age, τ_{CI} or τ_{CIE} is related to a difference between the values of α_{inj} (column (3) of Table 3), α_{CI} or α_{CIE} (columns 4 and 7 of Table 4). As this was noted in paper of Machalski et al. (2007), α_{inj} values derived with DYNAGE are usually lower than those fitted with SYNAGE. An opposite situation is rare; an example is the NE lobe of J1155+4029 for which the SYNAGE fit gave $\alpha_{\text{CI}} = 0.537 \pm 0.021$ and $\alpha_{\text{CIE}} = 0.580^{+0.13}_{-0.05}$ while $\alpha_{\text{inj}} = 0.615 \pm 0.019$ is found in this paper. Such a case is likely caused by a very uncertain observational data at low frequencies. In general, an increase of the difference $\alpha_{\text{syn}} - \alpha_{\text{inj}}$ corresponds to an increase of the ratio t/τ_{syn} , where the label 'syn' indicates either α_{CI} or α_{CIE} . This correlation (shown in Fig. 6) is strong; the correlation coefficient between the above two variables for our twenty lobes is $+0.837$ in the case of t/τ_{CI} and $+0.884$ in the case of t/τ_{CIE} . The data in Table 4 show that in 13 of 20 investigated lobes the synchrotron age calculated with $k=1$ and $m=-2$ is higher than the dynamical age determined in this paper (the ratio t/τ_{CIE} is less than unity in Fig. 6). Indeed, the corresponding factors in the KDA model of the jet's dynamics, given by equations (2) and (5), are $k=6/7$ and $m=-11/14$ for the assumed values of β , Γ_{B} , and Γ_{c} . As a result, we rather would expect $\tau_{\text{CIE}} = (10/7) \tau_{\text{CI}}$ instead of $\tau_{\text{CIE}} = 4 \tau_{\text{CI}}$. In fact, in Fig. 6 the y-intercepts of t/τ_{CI} and

Table 4. Dynamical and synchrotron ages of the lobes

Source	Lobe	B_{DYN} (nT)	α_{CI}	$\nu_{\text{br,CI}}$ (GHz)	τ_{CI} (Myr)	α_{CIE}	$\nu_{\text{br,CIE}}$ (GHz)	τ_{CIE} (Myr)	$\alpha_{\text{CI}} - \alpha_{\text{inj}}$	$\alpha_{\text{CIE}} - \alpha_{\text{inj}}$	t/τ_{CI}	t/τ_{CIE}
(1)	(2)	(3)	(4)	(5)	(6)	(7)	(8)	(9)	(10)	(11)	(12)	(13)
J0912+3510	S	0.16	0.717	18.87	15.3	0.528	4.97	119.	0.224	0.010	5.88	0.76
	N	0.16	0.637	8.21	23.1	0.503	4.91	120.	0.150	0.016	3.24	0.63
J0927+3510	SE	0.18	0.684	3.74	14.4	0.541	1.63	87.2	0.194	0.051	2.85	0.47
	NW	0.14	0.434	0.30	45.7	0.554	1.77	75.3	-0.064	0.056	1.09	0.66
J1155+4029	SW	0.34	0.914	15.36	15.3	0.758	4.29	68.4	0.344	0.188	8.47	1.90
	NE	0.62	0.537	0.11	103.	0.580	(0.046)	(636)	-0.078	-0.035	1.15	0.19
J1313+6937	SE	0.23	0.613	2.54	70.4	0.490	0.82	496.	0.105	-0.018	2.16	0.31
	NW	0.28	0.643	4.29	116.	0.477	0.72	519.	0.132	-0.034	1.13	0.25
J1343+3758	NE	0.08	0.571	2.31	35.9	0.502	1.59	173.	0.110	0.041	1.78	0.37
	SW	0.11	0.646	1.51	50.8	0.681	6.99	94.5	0.130	0.165	1.85	1.00
J1453+3308	S	0.25	0.611	0.94	75.2	0.656	4.25	141.	0.048	0.093	2.30	1.23
	N	0.26	0.544	0.71	86.8	0.592	2.47	186.	0.026	0.074	1.46	0.68
J1604+3438	E	0.21	0.582	1.39	54.5	0.541	1.89	187.	0.076	0.035	1.58	0.46
	W	0.21	0.584	1.42	53.9	0.528	1.50	210.	0.073	0.017	1.72	0.44
J1604+3731	NW	0.35	0.769	1.59	14.4	0.783	3.27	40.1	0.198	0.212	3.75	1.35
	SE	0.35	0.702	1.48	14.9	0.732	5.13	32.0	0.166	0.196	2.75	1.28
J1702+4217	SW	0.32	0.665	1.49	32.9	0.668	4.97	72.2	0.097	0.100	2.25	1.03
	NE	0.27	0.668	2.14	26.6	0.617	3.99	77.9	0.130	0.079	2.33	0.80
J2312+1845	NE	0.71	0.783	4.08	19.0	0.656	3.27	85.0	0.216	0.089	4.52	1.01
	SW	0.76	0.770	4.06	18.3	0.617	2.29	97.3	0.203	0.050	4.16	0.78

**Figure 4.** Exemplary radio spectra of the lobes and fits of the three models of energy losses: CI (a pure continuous injection) – the solid line, original CIE (continuous injection and expansion – the dashed line, and DYNAGE – the dotted line. The values of α_{inj} fitted for each of the models and the corresponding reduced χ^2 values are given for a comparison.

t/τ_{CIE} at $\alpha_{\text{syn}} - \alpha_{\text{inj}} = 0$ differ by ~ 2 , not by 4. Therefore, we argue that the CI model underestimates the lobe's age since it does not take into account the expansion losses, while the CIE one overestimates the lobe's age since the original expansion factors ($k=1$ and $m=-2$) are likely too extreme. In between of these, the DYNAGE age solution should be better since the expansion parameters are connected to actual geometry of the lobes for each specific GRGs.

The plot in Fig. 6 shows that the dynamical age of the GRG's lobes is about 1 to 5 times larger than their radiative age. Very similar age ratios were found by Parma et

al. (1999) for much smaller, low luminosity radio galaxies. Beside the causes of this effect already discussed in the literature, there are two other possible explanation of this effect:

(1) As expected, both the synchrotron and the dynamical ages are sensitive to the α_{inj} parameter. However, it seems that an α_{inj} value determined with the DYNAGE method from the minimum kinetic energy of the jets is less sensitive to an uncertainty of the low-frequency spectrum of a source than values of α_{CI} or α_{CIE} found with SYNAGE. The only difference between the spectra provided with the model accounting for the adiabatic losses and the model not

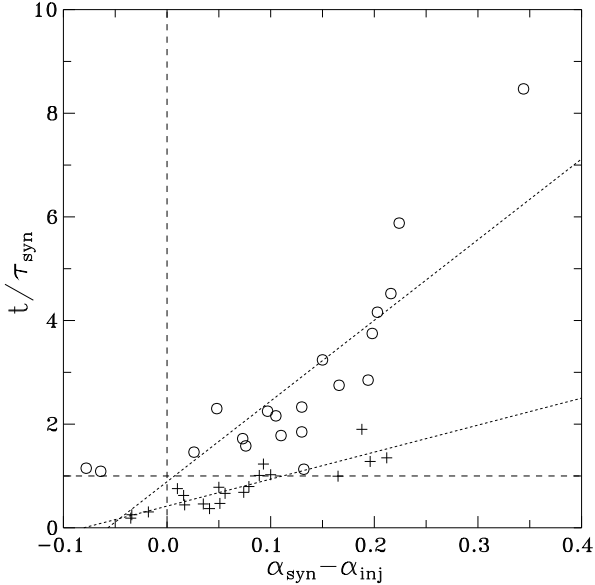


Figure 6. Ratio of the dynamical age of the lobes, t , and their synchrotron age, τ_{syn} , vs. the difference between $\alpha_{\text{syn}} - \alpha_{\text{inj}}$ where α_{syn} means either α_{CI} or α_{CIE} . The circles indicate the ratio of t and τ_{CI} while the crosses – the ratio of t and τ_{CIE} . The two dotted lines show linear regression lines of the above ratios on the $\alpha_{\text{syn}} - \alpha_{\text{inj}}$ coordinate.

accounting for them – is a larger range of transition of the spectral slope from α_{inj} to $\alpha_{\text{inj}} + 0.5$ in the former model. Therefore, in further discussion given below, we do not differentiate between α_{CI} and α_{CIE} . The α_{inj} and α_{CI} parameters both determine the slope of the spectrum at frequencies where radiative losses are not yet important.

In the classical spectral ageing analysis the CI model includes the continuum injection of relativistic particles having all the time the same power-law energy distribution. In the presence of energy losses due to magnetic fields the observed spectrum, being a sum of the emission from the various particle populations at different synchrotron ages, is characterized by a curvature between its low-frequency and high-frequency ends. This curvature is formed by many spectra with different normalizations and break frequencies. Implicit in this model is the assumption that the field strength is the same in the region of injection as in the outflow region. But the DYNAGE model is different because it accounts for the evolution of the magnetic field strength in a different way than the original CIE model does that. Hence the spectra calculated with it have different curvature. Probably the actual spectra have some curvature in them as well. SYNAGE cannot cope with such a curvature, thus fits a spectrum, single-broken between values of an α_{CI} and $\alpha_{\text{CI}} + 0.5$, to the data points. However, because the observed spectrum is already affected by radiative losses below the fitted break, α_{CI} (and α_{CIE}) comes out rather steep. Contrary to that, DYNAGE can cope with the above curvature because, basing on a more realistic model of dynamical expansion of the source (cocoon), it can better predict its spectrum. Therefore it can fit an aged spectrum with a flatter α_{inj} , because the part of the spectrum already affected by radiative losses extends to much lower frequencies than in the case of the classical ap-

proach. However, it should be noted that the KDA model for the cocoon’s emission is based on the approximation of the synchrotron kernel radiation with a ‘delta’-function. This approximation could artificially enhanced the spectral curvature, in the sense that it could result much more pronounced than it really is.

Resuming, we argue that usually DYNAGE, finding a flatter α_{inj} , is also less sensitive to its exact value. In other words, DYNAGE can afford radiative effects at lower frequencies than SYNAGE. Radiative effects at lower frequencies means older age, thus one can suspect that this effect is stronger at older ages than at younger ages where the spectra tend to be ‘straighter’, i.e. with only a single break and less curvature. But our, though very limited, statistics shows something else. The difference $\alpha_{\text{CIE}} - \alpha_{\text{inj}}$ seems to depend on redshift but not on the age. The correlation coefficient in the correlation between this difference and the redshift is $+0.63$. Again, this effect can support our thesis that DYNAGE can better afford radiative losses at low frequencies, where an intrinsic spectral curvature is shifted by the redshift, than the classical spectral ageing analysis.

(2) There is another factor having an influence on the difference between t and τ . This is the axial ratio R_{T} . Note that in the classical energy equipartition formula, $B_{\text{eq}} \propto (L/V_{\text{c}})^{2/7}$, the cocoon’s (lobe’s) volume is completely insensitive of a value of R_{T} what originate from the spherical geometry assumed in the classical formula of Pacholczyk (1970). Oppositely, because of the cylindrical geometry assumed in KDA and DYNAGE, the cocoon’s volume is strictly dependent of R_{T} which is $V_{\text{c}} \propto R_{\text{T}}^{-2}$ (its length D is measured much more precisely than the transversal base diameter). A variation of R_{T} results in a change of the pressure ratio \mathcal{P}_{hc} which determines the lobe (cocoon) energy density. This, in turn, specifies the magnetic field strength via the magnetic energy density (cf. equations (3), (4), and (5)). The data in Tables 3 and 4 confirm that the smaller the differences $\alpha_{\text{CIE}} - \alpha_{\text{inj}}$ (and closer to unity the ratio between magnetic field strength calculated with the formula of Miley (1980) and the field determined with equation (5) in this paper, B_{DYN}), the closer the dynamical and radiative ages.

6 ACKNOWLEDGEMENTS

J.M. thanks Dr. Christian R. Kaiser for helpful discussions and constructive suggestions, and the anonymous referee for the criticism which allowed us to improve the paper. JM and MJ acknowledge the MNiSW funds for scientific research in years 2005-2007 under contract No. 0425/PO3/2005/29.

REFERENCES

- Alexander, P., Leahy J.P., 1987, MNRAS, 225, 1
- Beck, R., Krause, M., 2005, Astron. Nachr., 6, 414
- Begelman, M.C., Cioffi, D.F., 1989, ApJ, 345, L21
- Blandford, R.D., Eichler, D., 1987, Phys. Rep., 154, 1
- Blundell, K.M., Rawlings, S., Willott, C.J., 1999, AJ, 117, 766
- Blundell, K.M., Rawlings, S., 2000, AJ, 119, 1111
- Brocksopp, C., Kaiser, C.R., Schoenmakers, A.P., de Bruyn, A.G., 2007, MNRAS, 382, 1019

- Carilli, C.L., Perley, R.A., Dreher, J.W., Leahy, J.P., 1991, *ApJ*, 383, 554
- Cohen, A.S., Lane, W.M., Cotton, W.D., Kassim, N.E., et al., 2007, *AJ*, 134, 1245
- Condon, J.J., Cotton, W.D., Greisen, E.W., Yin, Q.F., et al., 1998, *AJ*, 115, 1693
- Eilek, J.A., Arendt, P.N., 1996, *ApJ*, 457, 150
- Falle, S.A.E.G., 1991, *MNRAS*, 250, 581
- Ficarra, A., Grueff, G., Tomassetti, G., 1985, *A&AS*, 59, 255
- Gopal-Krishna, Wiita, P.J., 1987, *MNRAS*, 226, 531
- Hardcastle, M.J., Cheung, C.C., Feain, I.J., Stawarz, L., 2008, [arXiv:0808.1593v1]
- Heavens, A.F., Meisenheimer, K., 1987, *MNRAS*, 225, 335
- Isobe, N., Makishima, K., Tashoro, M., Itoh, K., et al., 2006, *ApJ*, 645, 256
- Jaffe, W.J., Perola, G.C., 1973, *A&A*, 26, 423
- Jamrozy, M., Konar, C., Machalski, J., Saikia, D.J., 2008, *MNRAS*, 385, 1286 (Paper II)
- Jones, T.W., Ryu, D., Engel, A., 1999, *ApJ*, 512, 105
- Kaiser, C.R., 2000, *A&A*, 362, 447
- Kaiser, C.R., Alexander, P., 1997, *MNRAS*, 286, 215 (KA)
- Kaiser, C.R., Dennett-Thorpe, J., Alexander, P., 1997, *MNRAS*, 292, 723 (KDA)
- Kardashev, N.S., 1962, *SvA*, 6, 317
- King, I.R., 1972, *ApJ*, 174, L123
- Kino, M., Kawakatu, N., 2005, *MNRAS*, 364, 659
- Klein, U., Mack, K.-H., Gregorini, L., Parma, P., 1995, *A&A*, 303, 427
- Konar, C., Saikia, D.J., Jamrozy, M., Machalski, J., 2006, *MNRAS*, 372, 693
- Konar, C., Jamrozy, M., Saikia, D.J., Machalski, J., 2008, *MNRAS*, 383, 525 (Paper I)
- Lacy, M., Rawlings, S., Saunders, R., Warner, P.J., 1993, *MNRAS*, 264, 721
- Lara, L., Mack, K.-H., Lacy, L., Klein, U., Cotton W.D., Feretti L., Giovannini G., Murgia M., 2000, *A&A*, 356, 63
- Leahy, J.P., Muxlow, T.W.B., Stephens, P.W., 1989, *MNRAS*, 239, 401
- Liu, R., Pooley, G., Riley, J.M., 1992, *MNRAS*, 257, 545
- Longair, M.S., Riley, J.M., 1979, *MNRAS*, 188, 625
- Machalski, J., Chyży, K.T., Stawarz, L., Koziel, D., 2007, *A&A*, 462, 43
- Machalski, J., Koziel-Wierzbowska, D., Jamrozy, M., Saikia, D.J., 2008, *ApJ*, 679, 149
- Mack, K.-H., Klein, U., O'Dea, C.P. Willis, A.G., Saripalli, L., 1998, *A&A*, 329, 431
- Manolakou, K., Kirk, J.G., 2002, *A&A*, 391, 127
- Miley, G.K., 1980, *ARA&A*, 18, 165
- Morganti, R., Killeen, N.E.B., Ekers, R.D., Oosterloo, T.A., 1999, *MNRAS*, 307, 750
- Murgia, M., 1996, Ph.D Laurea Thesis, University of Bologna
- Myers, S.T., Spangler, S.R., 1985, *ApJ*, 291, 52
- Nath, B.B., 1995, *MNRAS*, 274, 208
- Owsianik, I., Conway, J.E., Polatidis, A.G., 1998, *A&A*, 336, L37
- Owsianik, I., Conway, J.E., 1998, *A&A*, 337, 69
- Pacholczyk, A.G., 1970, *Radio Astrophysics*, Freeman, San Francisco
- Parma, P., Murgia, M., Morganti, R., Capetti, A., de Ruiter H.R., Fanti R., 1999, *A&A*, 344, 7
- Pooley, D.M., Waldram, E.M., Riley, J.M., 1998, *MNRAS*, 298, 637
- Rengelink, R.B., Tang, Y., de Bruyn, A.G., Miley, G.K., et al., 1997, *A&AS*, 124, 259
- Riley, J.M.W., Waldram, E.M., Ruley, J.M., 1999, *MNRAS*, 306, 31
- Rudnick, L., Katz-Stone, D., Anderson, M., 1994, *ApJS*, 90, 955
- Saripalli, L., Subrahmanyam, R., Hunstead R. W., 1994, *MNRAS*, 269, 37
- Saripalli, L., Subrahmanyam, R., Shankar, N.U., 2002, *ApJ*, 565, 256
- Scheuer, P.A.G., 1974, *MNRAS*, 166, 513
- Schoenmakers, A.P., Mack, K.-H., Lara, L., Röttgering, H.J.A., de Bruyn, A.G., van der Laan, H., Giovannini, G., 1998, *A&A*, 336, 455
- Schoenmakers, A.P., Mack, K.-H., de Bruyn, A.G., Röttgering, H.J.A., Klein, U., van der Laan, H., 2000, *A&AS*, 146, 293
- Tashiro, M., Aneda, H.K., Akishima, K.M., Iyomoto, N., et al., 1998, *ApJ*, 499, 713
- Tashiro, M., Isobe, N., Seta, H., Matsuta, K., et al., 2008, [arXiv:0809.2448v1]